Materials Science and Engineering A 517 (2009) 24–29

Contents lists available at ScienceDirect

Materials Science and Engineering A

journal homepage: www.elsevier.com/locate/msea

Dynamic testing at high strain rates of an ultrafine-grained magnesium alloy processed by ECAP

B. Li[a,*], S. Joshi[a,e], K. Azevedo[a], E. Ma[a], K.T. Ramesh[a], R.B. Figueiredo[b,c], T.G. Langdon[b,c,d]

[a] Center for Advanced Metallic and Ceramic Systems, The Johns Hopkins University, Baltimore, MD 21218, USA
[b] Department of Aerospace and Mechanical Engineering, University of Southern California, Los Angeles, CA 90089-1453, USA
[c] Department of Materials Science, University of Southern California, Los Angeles, CA 90089-1453, USA
[d] Materials Research Group, School of Engineering Sciences, University of Southampton, Southampton SO17 1BJ, UK
[e] Department of Mechanical Engineering, National University of Singapore, Singapore 117576, Singapore

ARTICLE INFO

Article history:
Received 27 December 2008
Received in revised form 11 March 2009
Accepted 12 March 2009

Keywords:
Dynamic testing
Equal-channel angular pressing
Magnesium alloy
Twinning
Ultrafine-grained structure

ABSTRACT

A ZK60 magnesium alloy was processed by equal-channel angular pressing (ECAP) at 473 K to produce a grain size of ~0.8 μm and it was then tested under dynamic conditions at strain rates up to 4.0×10^3 s^{-1} using a split-Hopkinson bar. The stress–strain curves in dynamic testing exhibited upwards concave curvature suggesting the occurrence of twinning. Examination by transmission electron microscopy showed that dislocation slip played a major role in the flow behavior with dislocation accumulation as the main source of work hardening. An identification of Burgers vectors revealed the extensive presence of prismatic dislocations. Rod-shaped $Mg_1(Zn,Zr)_1$ precipitates present in the as-received alloy become fragmented and overaged during ECAP.

1. Introduction

Magnesium alloys have received considerable attention in recent years because of their low density and high specific strength. These alloys are attractive engineering materials for use in a wide range of aerospace, automotive and other applications and also they are potential candidate materials for use in armor applications. Nevertheless, the relatively low strength of Mg alloys has hindered their utilization and accordingly considerable effort has been expended in recent research to exploring approaches that may be used to attain higher strength.

Grain refining is an effective procedure for achieving both high strength and reasonable ductilities at room temperature together with possible superplastic forming capabilities at elevated temperatures. It is well established that the application of severe plastic deformation (SPD) is effective in producing significant grain refinement in many metals [1] and this may be achieved using procedures such as equal-channel angular pressing (ECAP) where a sample is pressed through a die constrained within a channel bent through a sharp angle [2]. Although ECAP may be applied relatively easily to achieve grain refinement in f.c.c. metals, it is less easy to use the same procedure with h.c.p. metals such as magnesium because the grain refinement is heterogeneous and markedly dependent upon the initial grain structure of the alloy [3]. Early experiments demonstrated the difficulty of attaining refinement to the submicrometer level in pure Mg and a magnesium alloy when pressing from the cast condition [4] but subsequently it was shown that bulk ultrafine-grained (UFG) Mg alloys may be achieved by using a two-step procedure in which the alloy is initially extruded prior to processing by ECAP [5]. This approach, termed EX-ECAP, has now been used successfully for achieving significant grain refinement in a range of magnesium-based alloys [6–11].

For many potential vehicular and armor applications, magnesium alloys should be examined under conditions of dynamic loading at room temperature using strain rates up to at least 10^3 s^{-1}, where these high rates may be used to evaluate the resistance to damage from the impact of foreign objects at high speeds. To date, only very limited information is available on the dynamic properties of any Mg alloys. For example, early research documented the mechanical properties of a WE43 (Mg–Y–Nd–Zr) alloy under dynamic loading using a modified Hopkinson pressure bar and described high energy absorption and an elongation to failure of ~20% [12]. There is also a later report describing high strain rate behavior in an extruded ZK60 (Mg–Zn–Zr) alloy where both the strength and ductility were improved at grain sizes down to ~2 μm [13]. Although these latter results are attractive, more recent

* Corresponding author. Tel.: +1 410 516 8934.
E-mail address: bli@jhu.edu (B. Li).

0921-5093/$ – see front matter © 2009 Elsevier B.V. All rights reserved.
doi:10.1016/j.msea.2009.03.032

experiments have shown that processing by ECAP may be used to achieve even smaller grain sizes, in the submicrometer range, in the ZK60 alloy [14–16].

Accordingly, the present investigation was initiated with two objectives. First, to process a commercial ZK60 alloy by ECAP to achieve a UFG structure and to test under dynamic loading at strain rates up to $4.0 \times 10^3\ s^{-1}$. Second, to provide a first report characterizing the microstructure and the deformation behavior of a magnesium alloy subjected to dynamic testing after ECAP.

2. Experimental material and procedures

The experiments were conducted using a commercial ZK60 alloy obtained from the Timminco Corporation (Aurora, CO) and containing, in wt%, Mg–5.5% Zn–0.5% Zr. The alloy was received in the form of extruded rods with diameters of 10 mm and an initial grain size of ~2.9 μm. The processing by ECAP was performed using billets with lengths of 60 mm which were pressed through a solid die having an angle between the two parts of the channel of $\Phi = 90^\circ$ and an outer arc of curvature at the intersection of the two parts of $\Psi \approx 20^\circ$. It can be shown that these values of Φ and Ψ lead to an imposed strain of ~1 on each pass through the die [17]. Repetitive pressings were conducted for 8 passes at a temperature of 473 K using processing route B_C in which every billet is rotated by 90° in the same sense between each pass [18].

Following ECAP, cylindrical and rectangular cuboid samples were cut from the billets using a wire electrical discharge machine (EDM) and these samples were lapped with a precision lapping fixture to give parallel end surfaces and variations in length of <5 μm over the longest dimension. The cylindrical specimens were used to record the stress–strain behavior and the cuboidal specimens were used to obtain photographic images during dynamic testing with a high-speed camera. Samples were prepared in two different configurations in which the loading axes were oriented: either longitudinal (parallel to the pressing direction) or transverse (in-plane, perpendicular to the pressing direction and parallel to the entry channel of the die). The circumferential surface was cut using a wire EDM and a special fixture was employed to ensure right circular cylindrical specimens. Quasi-static tests were conducted for comparison purposes and in these tests the interfaces between the specimens and the pressure bars were lubricated with a mixture of grease and an MoS_2 powder lubricant to reduce the frictional effects.

Compression Kolsky bar (or split-Hopkinson pressure bar) tests [19] were conducted to obtain the compressive response at high strain rates up to $>10^3\ s^{-1}$. The cylindrical specimens were 5 mm in diameter and with a length-to-diameter ratio of 0.6 in accordance with standard practice for metallic specimens in the Kolsky bar tests. The cuboidal specimens had a square cross-section of 4 mm × 4 mm with a similar height-to-width ratio. For both configurations, the interfaces between the specimens and the bars were adequately lubricated as in the quasi-static tests. A digital high-speed camera (DRS Hadland Ultra 8), with the ability to record eight frames at a rate of 10^8 frames per second, was synchronized with the Kolsky bar system to record the deformation and failure of the specimens in dynamic loading. The cuboidal specimens were polished on one rectangular surface to a mirror-like finish and this surface was used to record images with the high-speed camera.

Transmission electron microscope (TEM) specimens were prepared from the untested and tested samples for microstructural examination. The specimens were mechanically polished down to ~130 μm on a series of sand papers down to 800 grit. Care was taken to avoid water contamination during the final polishing. Disks of 3 mm diameter were then mechanically punched out of the polished samples and these disks were polished using a Tenupol-3 electropolisher. After electropolishing, the specimens were cleaned by ion-milling for ~0.5 h using gentle conditions of a low incident angle and a low voltage. Liquid nitrogen was applied during the ion-milling. The electron-transparent specimens were examined using a Philips 420 TEM at an accelerating voltage of 120 kV.

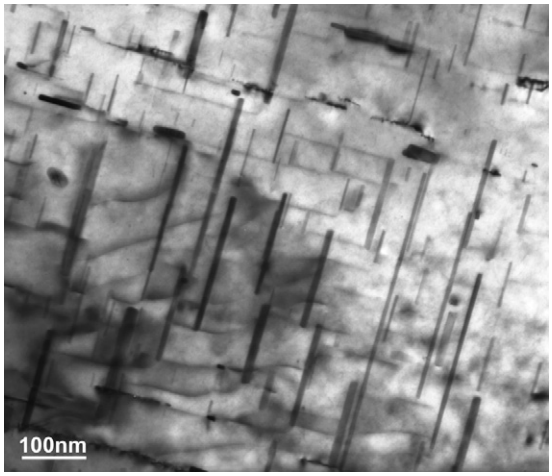

Fig. 1. Microstructure of the extruded ZK60 Mg alloy showing the presence of rod-shaped precipitates.

Energy dispersive X-ray spectroscopy (EDS) was performed using a nano-sized beam in a high resolution TEM in order to reduce the excitation volume and identify the precipitates in the UFG ZK60 alloy. The measured spectra were compared directly with the spectra obtained from the as-received extruded alloy.

3. Experimental results

3.1. Microstructural characteristics

Fig. 1 shows a TEM micrograph of the microstructure of the commercial extruded as-received ZK60 alloy. It is apparent that many precipitates are present and many of these precipitates are rod-shaped although some spherical particles are also visible. There is also evidence for some dislocation interactions with the rod-shaped precipitates in this initial extruded condition.

Examples of the microstructures of the UFG ZK60 alloy processed through 8 passes by ECAP are shown in Fig. 2. In Fig. 2(a) at the lower magnification, there is a distribution of reasonably equiaxed grains with a measured average grain size of ~0.8 μm. In this condition the grain boundaries appear to have predominantly high-angles of misorientation and this is consistent with the high superplastic elongations that are a feature of this alloy when testing in tension at elevated temperatures [16]. Fig. 2(b) shows a higher magnification and the arrow denotes a row of dislocations which appear to separate a grain into sub-grains.

It is important to note from the TEM images in Fig. 2 that processing by ECAP changes the morphology of the precipitates. Whereas there is evidence for many rod-shaped precipitates in the as-received condition in Fig. 1, after ECAP in Fig. 2 the precipitates are generally spherical with sizes below ~100 nm and with a reasonably uniform distribution both throughout the grains and along the grain boundaries. The nature of the precipitates was analyzed by EDS in both the extruded condition and after ECAP and the results are shown in Fig. 3. In the extruded condition shown in Fig. 3(a) the majority of the rod-shaped precipitates are identified as $Mg_1(Zn,Zr)_1$, whereas after ECAP shown in Fig. 3(b) the rounded particles are $Mg_1(Zn,Zr)_1$ and Mg_1Zn_1.

3.2. High strain rate compression testing

An example of dynamic testing is shown in Fig. 4 for a cuboidal specimen tested at a rate of $2.0 \times 10^3\ s^{-1}$. The plot shows true

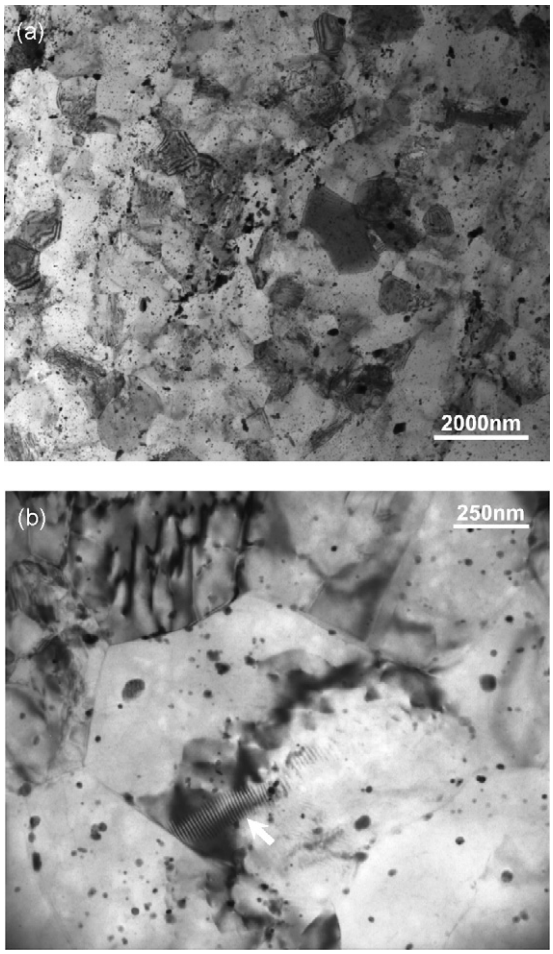

Fig. 2. Characterization of the microstructure after ECAP at (a) low and (b) high magnifications: the grain size was measured as ~800 nm.

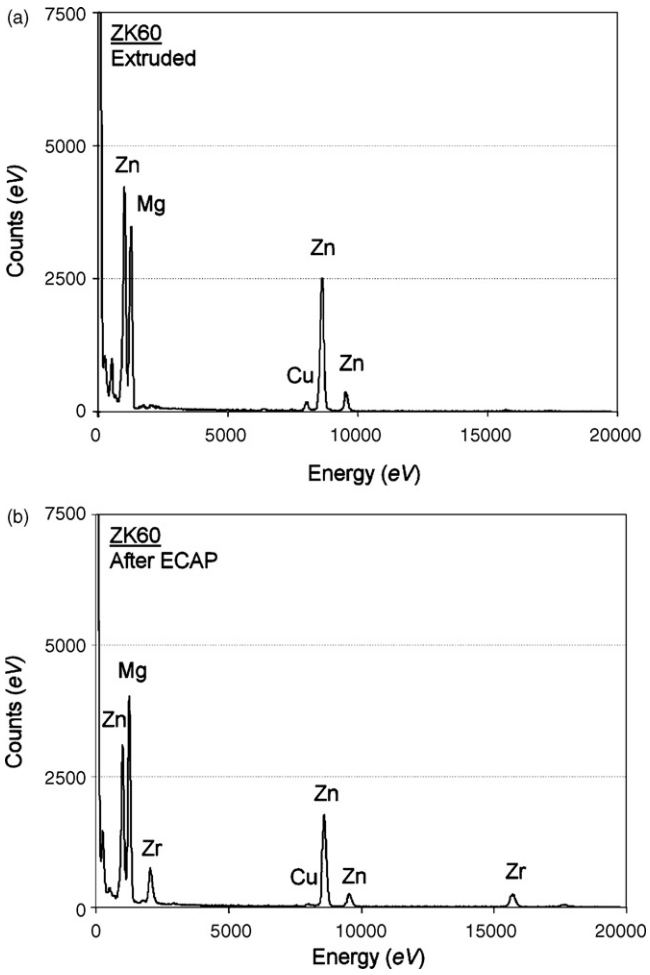

Fig. 3. An EDS analysis of precipitates in the ZK60 alloy (a) in the extruded condition and (b) after processing by ECAP.

stress versus time and superimposed are a series of digital images recorded on the specimen surface at different stages of the dynamic testing and captured using the high-speed camera. These images reveal the presence of shear bands at the higher strains and it is apparent that these bands lead ultimately to failure of the sample.

Representative plots of true stress versus true strain in compression are shown in Fig. 5 for both the longitudinal (L) and transverse (T) samples using a series of strain rates from a quasi-static test at $1.0 \times 10^{-3}\ s^{-1}$ to dynamic testing up to $4.0 \times 10^{3}\ s^{-1}$. Inspection of these curves shows that the initial flow stress exhibits only a very minor dependence on strain rate whereas the rate of strain hardening and the ultimate strength are strain rate dependent. For the in-plane dynamic tests labeled L, the initial flow stresses are consistently of the order of ~200–230 MPa. There is also an apparent upper yield point and an inflection of the curve in the dynamic tests conducted at very rapid strain rates.

Considering the longitudinal and transverse tests conducted at the fastest strain rate, it is apparent that the initial flow stresses are similar at ~210 MPa and the flow stresses are similar, ~340–360 MPa, at high strains of ~0.15. However, despite this overall similarity, the curvature of the stress–strain curve is markedly different for the transverse specimen.

Although the longitudinal response of the UFG ZK60 alloy at dynamic strain rates is reasonably similar for the different strain rates, Fig. 5 shows that the peak stress increases at the higher strain rates. Furthermore, the strain hardening rate for each sample is readily divisible into two stages where there is a stage I from yielding to a strain level of ~7.5% in which the rate of hardening is relatively low and then a stage II from ~7.5% to failure in which there is an increasing rate of strain hardening. By contrast, for the transverse specimen the behavior is different because the rate of strain hardening is gradually reduced throughout the test.

3.3. Dislocation structures after high strain rate deformation

Fig. 6 shows examples of the dislocation structures after dynamic testing of an in-plane sample at $4.0 \times 10^{3}\ s^{-1}$. These and

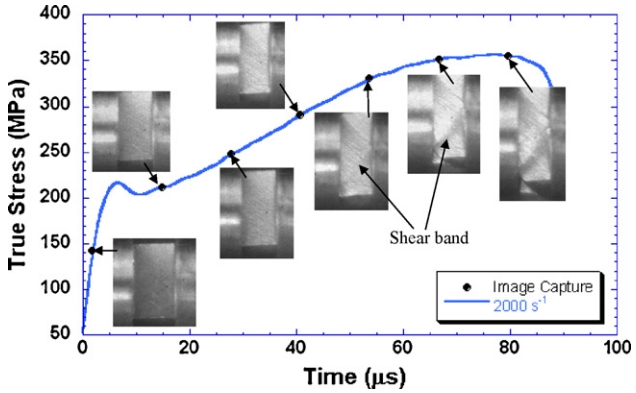

Fig. 4. A plot of true stress against time for a sample tested dynamically at a rate of $2 \times 10^{3}\ s^{-1}$: the digital images were recorded using a high-speed camera and they reveal the development of shear bands in the later stages of deformation.

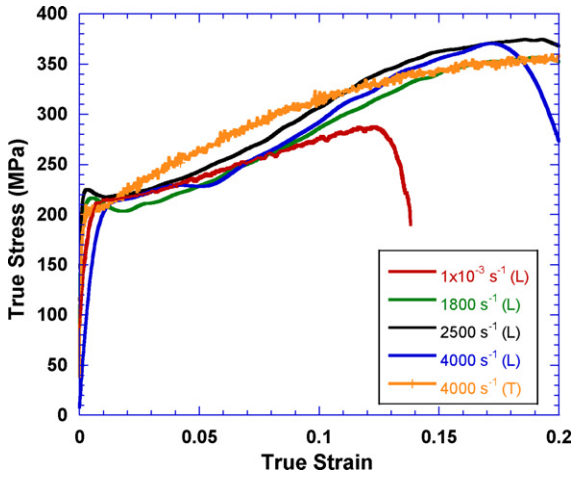

Fig. 5. Plots of true stress versus true strain for the ZK60 alloy processed by ECAP and tested in compression under quasi-static or dynamic conditions: the labels L and T denote testing in the longitudinal direction (parallel to the pressing direction) and the transverse direction (in-plane, parallel to the entry channel).

other similar observations showed that the dislocation density in these samples is extremely high. Fig. 6(a) depicts a high density of dislocations, very clear evidence for dislocation interactions and extensive dislocation tangles. The arrow in Fig. 6(a) shows an example of three arrays of dislocations impinging upon each other and thereby creating a lock that will serve as an obstacle to further dislocation slip. There is a well-defined dislocation network in Fig. 6(b) and the arrow marks an example of a dislocation pile-up against a precipitate located in a grain boundary.

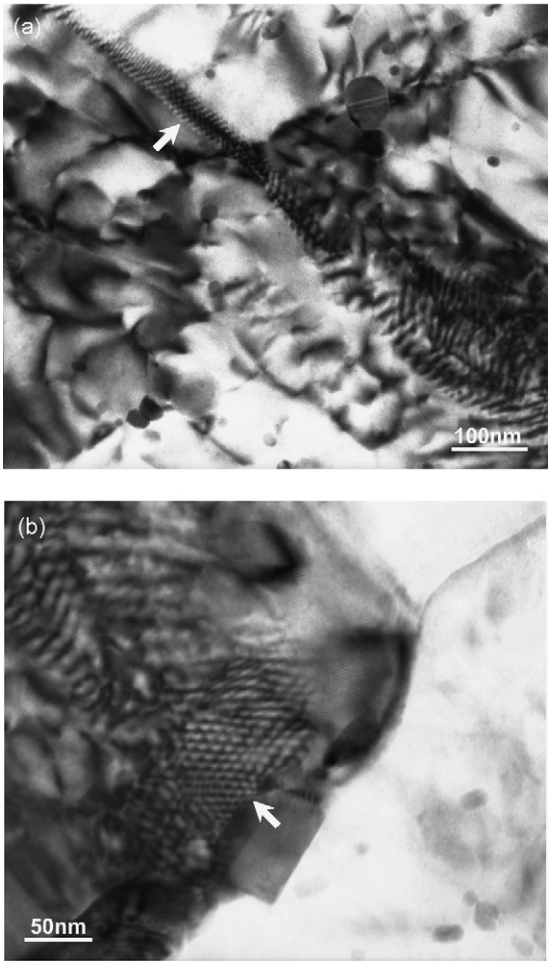

Fig. 6. Representative dislocation structures in the ZK60 alloy after dynamic testing at a strain rate of $4.0 \times 10^3\ s^{-1}$: the arrow in (a) shows three arrays of dislocations impinging together and the arrow in (b) shows a dislocation pile-up against a precipitate in a grain boundary.

4. Discussion

4.1. Nature of the precipitate morphology

An important first conclusion from this work is that the rod-shaped precipitates visible in the extruded condition in Fig. 1 are absent after processing by 8 passes of ECAP as shown in Fig. 2. Thus, the imposition of a high hydrostatic stress in ECAP at 473 K has a major effect on the nature of the precipitate morphology.

There is evidence from experiments conducted on an aluminum alloy that processing by ECAP at an elevated temperature may lead to significant precipitate fragmentation [20,21]. However, the ZK60 alloy is a precipitation-hardening magnesium alloy having zinc as its main alloying element. Furthermore, the precipitation kinetics of Mg–Zn alloys is well documented [22–26] and results are also available for the ZK60 alloy [27]. Thus, the main precipitate in this system is Mg_1Zn_1 which may occur as a transition phase (Mg_1Zn_1') with a rod-shaped configuration lying perpendicular to the basal plane or as an equilibrium phase (Mg_1Zn_1) with a disk shape lying parallel to the basal plane [22–26]. Since basal slip is the primary slip system, the former will constitute a more efficient obstacle for dislocations and thus a peak strength is anticipated when the majority of precipitates occur as Mg_1Zn_1'. The transition phase precipitates form in the early stages of aging and they may change into the equilibrium phase due to overaging. Since the present results show that rod-shaped precipitates are present in the extruded alloy but not after processing by ECAP at 473 K, it is reasonable to conclude that the ZK60 alloy undergoes overaging during ECAP. This is reasonable considering both the high temperature used for ECAP and the high imposed strains which will generate excess vacancies [28] and may thereby accelerate the aging process. The smaller size of the precipitates after ECAP suggests that the initial rod-shaped precipitates are also fragmented prior to overaging, and this is consistent with data reported for an aluminum 7034 alloy where precipitate fragmentation occurred primarily in the first pass of ECAP [20,21]. Finally, it should be noted that the change in the precipitates from Mg_1Zn_1' to Mg_1Zn_1 will reduce the strength of the alloy because the latter precipitate is a less efficient obstacle for dislocation motion on the basal planes.

4.2. The occurrence of twinning in the ZK60 alloy

The stress–strain curves in Fig. 5 for the quasi-static and dynamic compression tests conducted in the longitudinal direction show relatively similar stress levels. Furthermore, the dynamic curves exhibit an upward concave appearance and this is generally considered as indicative of the occurrence of twinning in Mg alloys [29–32] and Zr [33]. For the quasi-static test the initial stress is similar but there is significantly less curvature, thereby leading to a lower flow stress at the high strains. By contrast, the dynamic test conducted in the transverse direction exhibits a downward concave appearance which is consistent with slip-controlled deformation.

The similar stress levels for the tests carried out at different strain rates in the longitudinal direction shows that the deformation mechanism in the initial stages of flow is relatively insensitive to strain rate and this is consistent with the assumption of a constant stress for the activation of twinning [34]. The lower rate of strain hardening observed in the quasi-static test suggests that there is less twinning under these conditions because the twin boundaries

will act as obstacles for dislocation slip and increase the strain hardening. This conclusion is reasonable because it is known that the tendency for twinning tends to increase with increasing strain rate [34].

The absence of any evidence for twinning when testing in the transverse direction may be explained by the orientation character of twinning in low symmetry materials such as magnesium alloys. Processing by ECAP is known to impose a preferential texture in magnesium alloys and this leads to a significant anisotropy in the mechanical behavior [35]. It is reasonable to anticipate, therefore, that the tendency for twinning will vary in a manner that is dependent upon the testing orientation. This is supported by the results in a fine-grained and coarse-grained magnesium alloy which exhibit different behavior depending on the orientation of the compression loading axis [31]. The difference in flow behavior is attributed to the occurrence of twining which is orientation dependent.

Although upward concave curvature is an inherent feature of the stress–strain curves and this is consistent with the occurrence of twinning in dynamic testing in the longitudinal direction, it is important to note that twinning generally becomes less prevalent when the grain size is reduced [33]. For example, experiments on the ZK60 alloy showed no evidence for twinning at a grain size of ~2 μm [36] and tensile tests on an AZ31 (Mg–3% Al–0.75% Zn–0.25% Mn) alloy suggested the role of twinning was minor by comparison with the effect of grain size [37]. There is evidence with the AZ31 alloy for twinning-controlled flow at room temperature for grain sizes as fine as 3 μm [29] but relatively little twinning when the grain size is ~1.4 μm [31]. Accordingly, in the present experiments on the ZK60 alloy where the grain size is only ~0.8 μm, it is reasonable to anticipate the overall role of twinning may be fairly minor.

4.3. Characteristic features of dynamic flow

It is apparent from Fig. 6 that the dislocation density is very high after dynamic deformation at very rapid strain rates. This high density hinders any measurements of the individual Burgers vectors because of the overlapping strain fields. Nevertheless, some information may be extracted from the microstructural observations.

There is evidence for abundant dislocation tangles in Fig. 6(a) and (b) there is a well-defined dislocation network of dislocations piled up against a precipitate in a grain boundary. These dislocations at different orientations make an angle of about 60° with each other thereby suggesting they are either basal ⟨*a*⟩ or prismatic ⟨*a*⟩ dislocations. If the dislocations are basal ⟨*a*⟩ type, then all three-slip systems on the basal plane must be activated within this grain. In the plastic deformation of polycrystalline materials, dislocation slip is activated preferentially in those grains having orientations that satisfy the critical resolved shear stress (CRSS). This means those slip systems favorably orientated with large Schmid factors are activated first. Hence, for the grain shown in Fig. 6(b), it is assumed that this high density of dislocations is of the prismatic ⟨*a*⟩ type. Practically, to distinguish the prismatic ⟨*a*⟩ from the basal ⟨*a*⟩ dislocations requires adequately selected zone axes and a weak-beam dark-field technique [38]. For instance, zone axes parallel to the basal plane such as $[2\,\bar{1}\,\bar{1}\,0]$ and $[0\,1\,\bar{1}\,0]$ may be used to image the dislocations. With these zone axes, the basal ⟨*a*⟩ dislocations lie roughly parallel to each other. In the present TEM observations, the density of the basal ⟨*a*⟩ dislocations was low.

These observations suggest that the pronounced strain hardening in the later stage of plastic deformation at the dynamic strain rates is probably due to the generation of new prismatic dislocations. As the dislocation density is drastically increased during dynamic testing, the portion of mobile dislocations decreases because of mutual interactions between dislocations thereby giving an increase in the stress required for further flow. The origin of the prismatic ⟨*a*⟩ dislocations may be explained by noting that the CRSS for basal ⟨*a*⟩ dislocation is very low [39] so that the basal ⟨*a*⟩ dislocations are generally considered as the main source of plastic strain [40,41]. However, if slip is restricted to the basal plane it fails to satisfy the von Mises criterion of at least five independent slip systems and therefore, in addition to limited twinning, cross-slip will activate ⟨*a*⟩ dislocations on the non-basal planes. It has been shown that the grain boundaries play a key role in the activation of non-basal slip due to compatibility effects and this means that the cross-slip region may extend to the entire grain volume when the grain size is reduced from ~50 to ~7 μm [42]. The dislocation structures shown in Fig. 6 provide evidence for the development of high stresses near precipitates and grain boundaries and this will also facilitate the activation of non-basal slip systems.

An earlier report documented an improved strength and ductility during the dynamic testing of a fine-grained ZK60 alloy compared to the coarse-grained structure and it was concluded that grain refinement is effective in introducing a high capacity for energy absorption during dynamic deformation [13]. Specifically, these experiments gave an initial flow stress of up to ~400 MPa when testing with an average grain size of ~4 μm. This result is important because of the potential for utilizing this alloy in vehicular or armor applications. Nevertheless, the present results show a reduced strength of ~210 MPa after ECAP despite the production of a significantly smaller average grain size of ~0.8 μm. This apparent discrepancy is due to the microstructural features present in the alloy after ECAP and especially with the change in the morphology of the precipitates due to the high imposed pressures and the occurrence of overaging.

5. Summary and conclusions

1. Billets of a commercial extruded ZK60 magnesium alloy were processed by equal-channel angular pressing for 8 passes at 473 K to refine the grain size to ~0.8 μm.
2. Compression tests were conducted under dynamic conditions at strain rates up to $4.0 \times 10^3\ s^{-1}$ using a split-Hopkinson bar. The resulting stress–strain curves exhibit an upwards concave curvature which is generally interpreted as indicative of the occurrence of twinning.
3. An examination of the precipitate morphology suggests the occurrence of fragmentation and overaging during ECAP due to the high hydrostatic stress imposed in ECAP and the relatively high pressing temperature.
4. An examination by transmission electron microscopy after high strain rate deformation reveals a very high dislocation density and the presence of both basal and prismatic dislocations.

Acknowledgements

Research at the University of Southern California was supported by the U.S. Army Research Office under Grant No. W911NF-08-1-0201.

References

[1] R.Z. Valiev, R.K. Islamgaliev, I.V. Alexandrov, Prog. Mater. Sci. 45 (2000) 103–189.
[2] R.Z. Valiev, T.G. Langdon, Prog. Mater. Sci. 51 (2006) 881–981.
[3] R.B. Figueiredo, T.G. Langdon, Mater. Sci. Eng. A 501 (2009) 105–114.
[4] A. Yamashita, Z. Horita, T.G. Langdon, Mater. Sci. Eng. A 300 (2001) 142–147.
[5] Z. Horita, K. Matsubara, K. Makii, T.G. Langdon, Scripta Mater. 47 (2002) 255–260.
[6] K. Matsubara, Y. Miyahara, Z. Horita, T.G. Langdon, Acta Mater. 51 (2003) 3073–3084.
[7] K. Matsubara, Y. Miyahara, Z. Horita, T.G. Langdon, Metall. Mater. Trans. 35A (2004) 1735–1744.
[8] Y. Miyahara, K. Matsubara, Z. Horita, T.G. Langdon, Metall. Mater. Trans. 36A (2005) 1705–1711.
[9] H.K. Lin, J.C. Huang, T.G. Langdon, Mater. Sci. Eng. A 402 (2005) 250–257.

[10] Y. Miyahara, Z. Horita, T.G. Langdon, Mater. Sci. Eng. A 420 (2006) 240–244.
[11] M. Furui, H. Kitamura, H. Anada, T.G. Langdon, Acta Mater. 55 (2007) 1083–1091.
[12] T. Mukai, T. Mohri, M. Mabuchi, M. Nakamura, K. Ishikawa, K. Higashi, Scripta Mater. 39 (1998) 1249–1253.
[13] T. Mukai, M. Yamanoi, H. Watanabe, K. Ishikawa, K. Higashi, Mater. Trans. JIM 42 (2001) 1177–1181.
[14] H. Watanabe, T. Mukai, K. Ishikawa, K. Higashi, Scripta Mater. 46 (2002) 851–856.
[15] R.B. Figueiredo, T.G. Langdon, Mater. Sci. Eng. A 430 (2006) 151–156.
[16] R.B. Figueiredo, T.G. Langdon, Adv. Eng. Mater. 10 (2008) 37–40.
[17] Y. Iwahashi, J. Wang, Z. Horita, M. Nemoto, T.G. Langdon, Scripta Mater. 35 (1996) 143–146.
[18] M. Furukawa, Y. Iwahashi, Z. Horita, M. Nemoto, T.G. Langdon, Mater. Sci. Eng. A 257 (1998) 328–332.
[19] H. Kolsky, Proc. Phys. Soc. Lond. 62B (1949) 676–700.
[20] C. Xu, M. Furukawa, Z. Horita, T.G. Langdon, Acta Mater. 51 (2003) 6139–6149.
[21] C. Xu, M. Furukawa, Z. Horita, T.G. Langdon, Acta Mater. 53 (2005) 749–758.
[22] J.B. Clark, Acta Metall. 13 (1965) 1281–1289.
[23] G. Mima, Y. Tanaka, Trans. Jpn. Inst. Met. 12 (1971) 71–75.
[24] G. Mima, Y. Tanaka, Trans. Jpn. Inst. Met. 12 (1971) 76–81.
[25] G. Mima, Y. Tanaka, Trans. Jpn. Inst. Met. 12 (1971) 323–328.
[26] L.Y. Wei, G.L. Dunlop, H. Westengen, Metall. Mater. Trans. 26A (1995) 1705–1716.
[27] H. Watanabe, K. Moriwaki, T. Mukai, T. Ohsuna, K. Hiraga, K. Higashi, Mater. Trans. 44 (2003) 775–781.
[28] M.J. Zehetbauer, G. Steiner, E. Schafler, A. Korznikov, E. Korznikova, Mater. Sci. Forum 503–504 (2006) 57–64.
[29] M.R. Barnett, Z. Keshavarz, A.G. Beer, D. Atwell, Acta Mater. 52 (2004) 5093–5103.
[30] S.-B. Yi, C.H.J. Davies, H.-G. Brokmeier, R.E. Bolmaro, K.U. Kainer, J. Homeyer, Acta Mater. 54 (2006) 549–562.
[31] Q. Yang, A.K. Ghosh, Acta Mater. 54 (2006) 5159–5170.
[32] X.Y. Lou, M. Li, R.K. Boger, S.R. Agnew, R.H. Wagoner, Int. J. Plast. 23 (2007) 44–86.
[33] C.N. Tome, I.J. Beyerlein, S.C. Vogel, D.W. Brown, R.J. McCabe, Acta Mater. 54 (2006) 2887–2896.
[34] M.A. Meyers, O. Vöhringer, V.A. Lubarda, Acta Mater. 49 (2001) 4025–4039.
[35] S.R. Agnew, J.A. Horton, T.M. Lillo, D.W. Brown, Scripta Mater. 50 (2004) 377–381.
[36] R. Lapovok, P.F. Thomson, R. Cottam, Y. Estrin, J. Mater. Sci. 40 (2005) 1699–1708.
[37] J.A. del Valle, F. Carreño, O.A. Ruano, Acta Mater. 54 (2006) 4247–4259.
[38] B. Li, E. Ma, K.T. Ramesh, Metall. Mater. Trans. A 39A (2008) 2607–2614.
[39] T. Obara, H. Yoshinaga, S. Morozumi, Acta Metall. 21 (1973) 845–853.
[40] A. Galiyev, R. Kaibyshev, G. Gottstein, Acta Mater. 49 (2001) 1199–1207.
[41] M.H. Yoo, J.R. Morris, K.M. Ho, S.R. Agnew, Metall. Mater. Trans. A 33 (2002) 813–822.
[42] J. Koike, T. Kobayahsi, T. Mukai, H. Watanabe, M. Suzuki, K. Maruyama, K. Higashi, Acta Mater. 51 (2003) 2055–2065.